J. Fluid Mech. (2014), *vol.* 754, *pp.* 98–121.
doi:10.1017/jfm.2014.387

Turbulent Schmidt number and eddy diffusivity change with a chemical reaction

Tomoaki Watanabe†, Yasuhiko Sakai, Kouji Nagata and Osamu Terashima

Department of Mechanical Science and Engineering, Nagoya University, Nagoya 464-8603, Japan

(Received 27 August 2013; revised 24 June 2014; accepted 27 June 2014;
first published online 30 July 2014)

We provide empirical evidence that the eddy diffusivity $D_{t\alpha}$ and the turbulent Schmidt number $Sc_{t\alpha}$ of species α ($\alpha = \mathrm{A}$, B or R) change with a second-order chemical reaction ($\mathrm{A} + \mathrm{B} \rightarrow \mathrm{R}$). In this study, concentrations of the reactive species and axial velocity are simultaneously measured in a planar liquid jet. Reactant A is premixed into the jet flow and reactant B is premixed into the ambient flow. An optical fibre probe based on light absorption spectrometry is combined with I-type hot-film anemometry to simultaneously measure concentration and velocity in the reactive flow. The eddy diffusivities and the turbulent Schmidt numbers are estimated from the simultaneous measurement results. The results show that the chemical reaction increases $Sc_{t\mathrm{A}}$; $Sc_{t\mathrm{B}}$ is negative in the region where the mean concentration of reactant B decreases in the downstream direction, and is positive in the non-reactive flow in the entire region on the jet centreline. It is also shown that $Sc_{t\mathrm{R}}$ is positive in the upstream region whereas it is negative in the downstream region. The production terms of axial turbulent mass fluxes of reactant B and product R can produce axial turbulent mass fluxes opposite to the axial gradients of the mean concentrations. The changes in the production terms due to the chemical reaction result in the negative turbulent Schmidt number of these species. These results imply that the gradient diffusion model using a global constant turbulent Schmidt number poorly predicts turbulent mass fluxes in reactive flows.

Key words: jets, reacting flows, turbulent mixing

1. Introduction

A turbulent flow with chemical reactions (Hill 1976) can be observed in various settings. For example, it appears in combustors, in chemical reactors, and in pollutants emitted into the atmosphere and ocean. Therefore, it is important to investigate the mechanism of chemical reactions in turbulence and to develop numerical methods to precisely predict the turbulent reactive flows. Recently, direct numerical simulations (DNS) have been applied to turbulent reactive flows to investigate chemical reactions and to verify numerical models (e.g. Mizobuchi *et al.* 2005; Fabregat *et al.* 2010; Lignell, Chen & Schmutz 2011). However, performing DNS of turbulent flows with complex chemical reactions at high Reynolds number or high Schmidt number is not feasible because of the high computational cost. In practice, the Reynolds-averaged

† Email address for correspondence: watanabe.tomoaki@c.nagoya-u.jp

approach and large-eddy simulation (Pitsch 2006) are widely used to predict turbulent flows. In the former approach, the Reynolds-averaged Navier–Stokes equations and the Reynolds-averaged scalar transport equations are solved using turbulent models. The Reynolds-averaged scalar transport equation for passive scalar Γ_α is given by

$$\frac{\partial \langle \Gamma_\alpha \rangle}{\partial t} + \frac{\partial}{\partial x_i}(\langle U_i \rangle \langle \gamma_\alpha \rangle) = \frac{\partial}{\partial x_i}\left(D_\alpha \frac{\partial}{\partial x_i} \langle \Gamma_\alpha \rangle \right) - \frac{\partial}{\partial x_i} \langle u_i \gamma_\alpha \rangle + \langle S_\alpha \rangle. \tag{1.1}$$

Here, $\langle\ \rangle$ denotes an ensemble average, U_i is the velocity component, D_α is the molecular diffusivity of species α, S_α is the production rate of Γ_α by chemical reactions and the summation convention is applied to the index i; u_i and γ_α are the fluctuating components of U_i and Γ_α, respectively, and are represented by $u_i = U_i - \langle U_i \rangle$ and $\gamma_\alpha = \Gamma_\alpha - \langle \Gamma_\alpha \rangle$. In (1.1), the mean production rate $\langle S_\alpha \rangle$ and the turbulent scalar flux term $\langle u_i \gamma_\alpha \rangle$ appear in unclosed form. Several closure models have been developed for the mean production rate (e.g. Toor 1969; Patterson 1981; Dutta & Tarbell 1989), and some have been verified using experimental data (e.g. Wang & Tarbell 1993; Komori, Kanzaki & Murakami 1994; Chornyi & Zhdanov 2010). However, the models for the turbulent mass flux for reactive scalars have not been investigated in detail. One of the most practical and widely used models for $\langle u_i \gamma_\alpha \rangle$ is the gradient diffusion model (e.g. Tominaga & Stathopoulos 2007; Combest, Ramachandran & Dudukovic 2011), in which $\langle u_i \gamma_\alpha \rangle$ is modelled by

$$\langle u_i \gamma_\alpha \rangle = -D_{t\alpha} \frac{\partial \langle \Gamma_\alpha \rangle}{\partial x_i}. \tag{1.2}$$

Here, $D_{t\alpha}$ is the eddy diffusivity of species α and is generally given by

$$D_{t\alpha} = \frac{\nu_t}{Sc_{t\alpha}}, \tag{1.3}$$

where ν_t is an eddy viscosity, which is given by another turbulence model, and $Sc_{t\alpha}$ is the turbulent Schmidt number of species α. The gradient diffusion model is used to predict the turbulent mass flux even for reactive scalars (Wang & Tarbell 1993; Veynante & Vervisch 2002). In general, $Sc_{t\alpha}$ is assumed to be a global constant parameter. Here $D_{t\alpha}$ and $Sc_{t\alpha}$ play a crucial role in the Reynolds-averaged approach using the gradient diffusion model.

Experimental measurements of $D_{t\alpha}$ and $Sc_{t\alpha}$ require simultaneously measuring velocity and diffusive scalar. In a non-reactive flow, measurements of $D_{t\alpha}$ and $Sc_{t\alpha}$ are not as difficult and have been made in various studies (e.g. Flesch, Prueger & Hatfield 2002; Yimer, Campbell & Jiang 2002; Feng *et al.* 2005, 2007). Because it is difficult to simultaneously measure velocity and concentration of reactive species in a turbulent reactive flow, surprisingly few measurements of $D_{t\alpha}$ have been made so far: the eddy diffusivity for reactive species has been measured by Bilger, Saetran & Krishnamoorthy (1991) in a scalar mixing layer in the gas phase and by Komori *et al.* (1993) in a scalar mixing layer in the liquid phase. The results of Bilger *et al.* (1991) were discussed in detail by Toor (1993). These studies have shown that $D_{t\alpha}$ changes with a chemical reaction. Nevertheless, we have only scanty information on the effects of chemical reaction on $D_{t\alpha}$ and $Sc_{t\alpha}$: only one reactive component has been measured in a liquid (Komori *et al.* 1993) and no measurements of $Sc_{t\alpha}$ have been reported so far.

In turbulent premixed flames, the gradient diffusion model (1.2) is known to be inappropriate because the turbulent flux does not often align with the mean gradient direction, resulting in negative eddy diffusivity. The turbulent diffusion in the direction opposite to the mean gradient direction (i.e. negative eddy diffusivity) is called counter-gradient diffusion. It has been theoretically predicted (Bray *et al.* 1981; Libby & Bray 1981) and observed in experiments (Shepherd, Moss & Bray 1982; Cheng & Shepherd 1991) and numerical simulations (Veynante *et al.* 1997; Nishiki *et al.* 2006; Chakraborty & Cant 2009) of turbulent premixed flames. In turbulent flames, chemical reactions greatly affect the flow field. The counter-gradient diffusion in premixed flames is related to the heat release and the change in density due to chemical reactions (Veynante *et al.* 1997). It is also well known that under the effect of body force, such as found in stratified flows, counter-gradient diffusion occurs (e.g. Hanazaki & Hunt 1996; Komori & Nagata 1996).

In this study, we simultaneously measure concentrations of all reactive species and axial velocity in a planar liquid jet with a second-order chemical reaction $\mathrm{A}+\mathrm{B}\rightarrow\mathrm{R}$, and we experimentally measure $D_{t\alpha}$ and $Sc_{t\alpha}$ for all scalar components. In our experiment, the heat release and the change in density due to the reaction can be neglected because the reactants are dilute, and the reactive species act as passive scalars. Furthermore, the two reactants A and B are separately supplied from jet and ambient flows, respectively. Thus, the reactive jet investigated in this study is entirely different from turbulent premixed flames. Although the two reactants, which act as passive scalars, are supplied in a non-premixed condition, we will show that $D_{t\alpha}$ and $Sc_{t\alpha}$ drastically change with a chemical reaction, even permitting counter-gradient mass transport. We also show that the eddy diffusivity expression can be ill-defined for the turbulent mass flux in a reactive flow because the mean concentration gradient becomes zero although the turbulent mass flux has a non-zero value.

2. Experiments

A schematic diagram of a planar liquid jet with a second-order chemical reaction is shown in figure 1. Liquids for the ambient flow and the jet flow are supplied to a test section through two head tanks. The jet flow is injected into the ambient flow through a rectangular nozzle of width $d=2$ mm and spanwise length 40 mm. The origin of the coordinate system is located at the centre of the nozzle. Here x and y are the axial and cross-stream directions, respectively, with z completing the coordinate system. The axial velocity of the jet flow, U_J, is set to 1.29 m s^{-1} at $x=0$ and the axial velocity of the ambient flow, U_M, is set to 0.073 m s^{-1} at $x=0$. Thus, the Reynolds number defined by $Re=(U_J-U_M)d/\nu$ is 2200, where ν is the kinematic viscosity. The Schmidt number based on the molecular diffusivity of the non-reactive species C is $Sc\approx 600$.

The second-order chemical reaction investigated in this study is represented by $\mathrm{A}+\mathrm{B}\rightarrow\mathrm{R}$. The reactants are 1-naphthol (A) and diazotized sulphanilic acid (B). The product is 4-(4′-sulphophenylazo)-1-naphthol (R) and is a monoazo dyestuff. The reaction rate constant of the chemical reaction is $k=12\,000$ (Bourne, Hilber & Tovstiga 1985). In this study, reactant A is premixed into the jet flow and reactant B is premixed into the ambient flow. These flows are then mixed in the test section and product R is produced by the chemical reaction. The initial concentrations of reactants A and B are $\Gamma_{\mathrm{A}0}=0.4$ mol m^{-3} and $\Gamma_{\mathrm{B}0}=0.2$ mol m^{-3}, respectively. Thus, the Damköhler number, defined by $Da=k(\Gamma_{\mathrm{A}0}+\Gamma_{\mathrm{B}0})d/(U_J-U_M)$, which is the ratio of the timescale of flow to that of chemical reaction, is 11.8. The chemical reaction

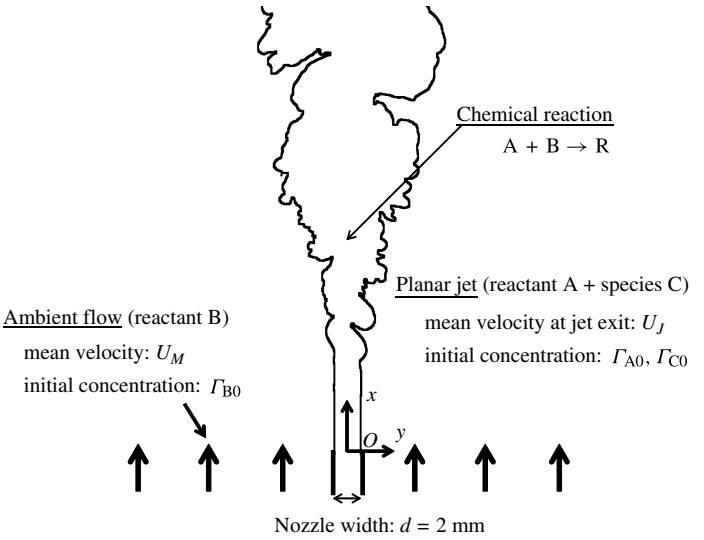

FIGURE 1. Planar jet with a second-order chemical reaction.

investigated in this study has a pH dependence. Therefore, we keep the pH in the flow constant by adding sodium carbonate and sodium hydrogen carbonate into the jet flow as buffer salts. To measure the concentrations of reactants A and B using conserved scalar theory (Bilger *et al.* 1991), acid blue 9 (species C) is also added into the jet flow. The species C is blue dyestuff, and it is independent of the chemical reaction. Therefore, the concentration of the non-reactive species C can be considered as a conserved scalar. Its initial concentration is $\Gamma_{C0} = 0.1$ kg m^{-3}. Because the reactants are dilute, the chemical reaction can be considered to be isothermal, and the reactive and non-reactive species (A, B, R and C) act as passive scalars.

3. Measurement methods

The axial velocity and the concentrations of the dyestuffs R and C are simultaneously measured by a combined probe (figure 2) consisting of an optical fibre probe and an I-type hot-film probe (TSI 1210-20W). Simultaneous measurement of instantaneous concentrations of the dyestuffs R and C is made using the optical fibre probe based on light absorption spectrometry (Nakamura, Sakai & Miyata 1987; Watanabe *et al.* 2012). The concentration measurement system is also shown in figure 2. The light from a halogen lamp is fed to the optical fibre probe through an optical fibre and passes through the measuring point. After the light passes the measuring point, it is split into two wavelengths ($\lambda_1 = 520$ nm and $\lambda_2 = 600$ nm) by a grating spectroscope and their light intensities are measured by a photomultiplier. When light of wavelength λ passes through a solution of one dyestuff species α, the light absorption spectrum is defined by

$$P(\lambda) \equiv -\ln \frac{I(\lambda)}{I_0(\lambda)}, \tag{3.1}$$

where $I_0(\lambda)$ is the intensity of incident light and $I(\lambda)$ is the instantaneous intensity of transmitted light. Beer's absorption law relates $P(\lambda)$ to the instantaneous concentration of species α, Γ_α, as follows:

$$P(\lambda) = k_\alpha(\lambda)\Gamma_\alpha. \tag{3.2}$$

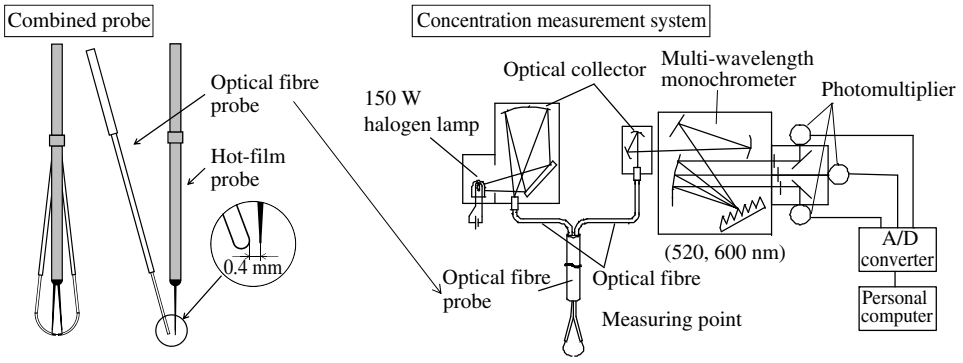

FIGURE 2. Measurement system.

Here, k_α is given by $k_\alpha = a_\alpha(\lambda)l$, where $a_\alpha(\lambda)$ depends on the absorptive characteristics of species α and l is the length of the light path. When light of wavelength λ passes through a solution of multiple dyestuff species, $P(\lambda)$ is equal to the sum of the $P(\lambda)$ for the solution of each species. Therefore, $P(\lambda_n)$ $(n = 1, 2)$ for the solution of the dyestuffs R and C is written as

$$P(\lambda_n) \equiv -\ln \frac{I(\lambda_n)}{I_0(\lambda_n)} = k_{\mathrm{R}}(\lambda_n)\Gamma_{\mathrm{R}} + k_{\mathrm{C}}(\lambda_n)\Gamma_{\mathrm{C}}. \tag{3.3}$$

Here $P(\lambda_n)$ for two wavelengths is measured by the optical fibre probe, and k_{R} and k_{C} are obtained from the calibration experiment. Hence, the instantaneous concentrations of dyestuffs R and C can be obtained from (3.3) by measuring $P(\lambda_1)$ and $P(\lambda_2)$.

The instantaneous concentrations of reactants A and B are calculated from the instantaneous concentrations of the dyestuffs R and C by using conserved scalar theory (Bilger *et al.* 1991) as follows:

$$\Gamma_{\mathrm{A}} = \xi\Gamma_{\mathrm{A0}} - \Gamma_{\mathrm{R}}, \tag{3.4}$$

$$\Gamma_{\mathrm{B}} = (1-\xi)\Gamma_{\mathrm{B0}} - \Gamma_{\mathrm{R}}. \tag{3.5}$$

Here, ξ is the mixture fraction defined by $\xi \equiv \Gamma_{\mathrm{C}}/\Gamma_{\mathrm{C0}}$; Γ_{R} and ξ are directly measured by the optical fibre probe. The instantaneous concentrations of reactants A and B are calculated from (3.4) and (3.5).

The mass conservation law is obtained from (3.4) and (3.5) as follows:

$$\frac{\Gamma_{\mathrm{A}}}{\Gamma_{\mathrm{A0}}} + \frac{\Gamma_{\mathrm{B}}}{\Gamma_{\mathrm{B0}}} + \frac{\Gamma_{\mathrm{R}}}{\Gamma_{\mathrm{R0}}} = 1, \tag{3.6}$$

where Γ_{R0} is defined by $\Gamma_{\mathrm{R0}} \equiv \Gamma_{\mathrm{A0}}\Gamma_{\mathrm{B0}}/(\Gamma_{\mathrm{A0}} + \Gamma_{\mathrm{B0}})$. In this study, $\Gamma_{\mathrm{R0}} = 0.133$ mol m^{-3}.

Bilger *et al.* (1991) introduced the frozen limit, which is the limiting case of no reaction ($Da \to 0$), and the equilibrium limit, which is the limiting case of infinitely fast reaction ($Da \to \infty$). The equilibrium limit has been used in the previous studies of a single-step chemical reaction (Bilger *et al.* 1991; Mell *et al.* 1994; Brown & Bilger 1998*a*,*b*; de Bruyn Kops, Riley & Kosaly 2001; Sawford 2006). In this study, the concentrations for the frozen limit, Γ_α^0, are derived as follows:

$$\Gamma_{\mathrm{A}}^0 \equiv \lim_{Da\to 0} \Gamma_{\mathrm{A}} = \xi\Gamma_{\mathrm{A0}}, \tag{3.7}$$

$$\Gamma_{\mathrm{B}}^{0} \equiv \lim_{Da\to 0} \Gamma_{\mathrm{B}} = (1-\xi)\Gamma_{\mathrm{B0}}, \tag{3.8}$$

$$\Gamma_{\mathrm{R}}^{0} \equiv \lim_{Da\to 0} \Gamma_{\mathrm{R}} = 0. \tag{3.9}$$

The concentrations for the equilibrium limit, Γ_{α}^{∞}, are derived as follows:

$$\Gamma_{\mathrm{A}}^{\infty} \equiv \lim_{Da\to\infty} \Gamma_{\mathrm{A}} = (\Gamma_{\mathrm{A0}} + \Gamma_{\mathrm{B0}})(\xi - \xi_S)H(\xi - \xi_S), \tag{3.10}$$

$$\Gamma_{\mathrm{B}}^{\infty} \equiv \lim_{Da\to\infty} \Gamma_{\mathrm{B}} = (\Gamma_{\mathrm{A0}} + \Gamma_{\mathrm{B0}})(\xi_S - \xi)H(\xi_S - \xi), \tag{3.11}$$

$$\Gamma_{\mathrm{R}}^{\infty} \equiv \lim_{Da\to\infty} \Gamma_{\mathrm{R}} = \begin{cases} \Gamma_{\mathrm{A0}}\xi & (\xi < \xi_S) \\ \Gamma_{\mathrm{B0}}(1-\xi) & (\xi \geqslant \xi_S). \end{cases} \tag{3.12}$$

Here, $H(z)$ is defined to be 0 for $z<0$ and 1 for $z\geqslant 0$; ξ_S is the stoichiometric ratio of the reactants in the mixture and is given by $\xi_S = \Gamma_{\mathrm{B0}}/(\Gamma_{\mathrm{A0}} + \Gamma_{\mathrm{B0}})$. In this study, $\xi_S = 0.333$. The results for the frozen limit ($Da \to 0$) and the equilibrium limit ($Da \to \infty$) are compared with the results for finite Damköhler number ($Da = 11.8$). It is noted that the results for the frozen limit are equivalent to those for the non-reactive species.

The combined probe consisting of the optical fibre probe and the I-type hot-film probe is used to simultaneously measure the axial velocity and the concentrations of the dyestuffs R and C. It was previously confirmed that a concentration fluctuation up to 2000 Hz can be accurately measured by using the concentration measurement system shown in figure 2 (Watanabe *et al.* 2012). The diameter of the optical fibre bundle used in the optical fibre probe is 0.5 mm and the length of the sampling volume is 0.7 mm. The length and the diameter of the sensing element of the I-type hot-film probe are 1.02 mm and 50.8 μm, respectively. The distance between two probes is 0.4 mm. The Kolmogorov scale η_K and the Taylor microscale λ_x are 0.427 mm and 2.32 mm at $x/d = 20$ on the jet centreline, respectively (Watanabe *et al.* 2012). The Batchelor scale, which is the smallest scale of scalar fluctuation, is $\eta_{\mathrm{B}} = \eta_K/Sc^{1/2} = 0.0174$ mm at $x/d = 20$ on the jet centreline. The spatial resolution of the combined probe is comparable to the Kolmogorov scale, and is much smaller than the Taylor microscale. It has been verified that simultaneous measurements of velocity and concentration can be accurately conducted using this combined probe in the same jet flow (Watanabe *et al.* 2012).

In this study, we mainly investigate the turbulent mass fluxes and the mean concentrations. As can be seen in the previous measurements of turbulent mass fluxes and cospectra of scalar and velocity fluctuations (Komori & Nagata 1996; Nagata & Komori 2000), the large-scale fluctuations make a much greater contribution to the turbulent mass flux than the small-scale fluctuations. Cospectra of axial velocity and concentration of the reactive species measured in the present experiment were shown in Watanabe *et al.* (2013). It was found that the large-scale fluctuations, which greatly affect the turbulent mass flux, are resolved well by the present measurement systems. Therefore, although the spatial resolution is larger than the Batchelor scale, it is sufficiently small for measuring the turbulent mass fluxes.

Concentration and velocity are simultaneously measured over $T = 21$ s, and the sampling frequency is 5000 Hz. The integral timescales of axial velocity and concentration of the non-reactive species C are about $T_U = 5 \times 10^{-3}$ s and $T_{\mathrm{C}} = 3 \times 10^{-3}$ s at $x/d = 20$ on the jet centreline, respectively. Thus, the measurement is conducted over a much longer time interval than the timescales of the large-scale fluctuations of the flow and scalar fields, indicating that a large number of

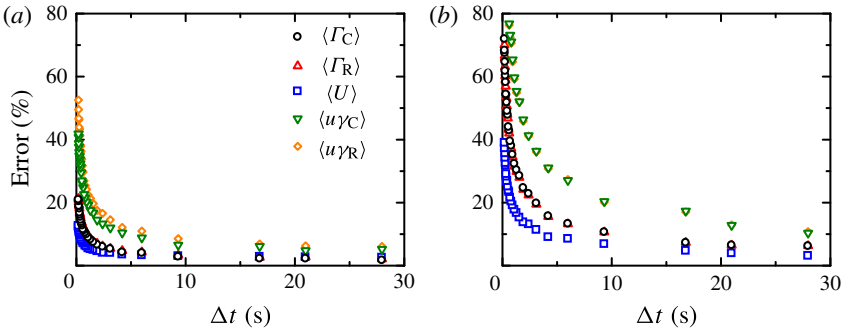

FIGURE 3. (Colour online) Convergence of statistics and uncertainty of the measurement. The statistics are calculated from the concentration and velocity signals measured over $T = 336$ s by taking the time average over various time intervals Δt. The r.m.s. values of the fluctuation of statistics from their mean values is shown. The r.m.s. values are normalized by the mean values of the statistics. (*a*) $x/d = 10$, (*b*) $x/d = 40$.

independent samples are used for calculating the statistics. The number of independent samples for velocity and concentration can be estimated as $N_U = T/(2T_U) = 2100$ and $N_C = T/(2T_C) = 3500$ (Tennekes & Lumley 1972). The relative errors in mean estimation (Tennekes & Lumley 1972) are $\sqrt{\langle u^2\rangle/(\langle U\rangle^2 N_U)} = 0.5\,\%$ and $\sqrt{\langle \gamma_C^2\rangle/(\langle \Gamma_C\rangle^2 N_C)} = 0.3\,\%$ for velocity and concentration, respectively.

To check the convergence of statistics, simultaneous measurements of concentration and velocity are conducted over $T = 336$ s at $x/d = 10$ and 40. The mean concentration of the non-reactive species C and product R ($\langle \Gamma_C\rangle$ and $\langle \Gamma_R\rangle$), the mean axial velocity ($\langle U\rangle$) and the axial turbulent mass flux of the non-reactive species C and product R ($\langle u\gamma_C\rangle$ and $\langle u\gamma_R\rangle$) are calculated by using the time average taken over various time intervals Δt. The measured signals of concentration and velocity are divided into $T/\Delta t$ blocks, each of which corresponds to the time interval Δt. The statistics based on the time average taken over Δt are calculated for each block. We use the root mean square (r.m.s.) values of the fluctuation of statistics from its mean value among all blocks for investigating convergence of statistics and uncertainty of the measurement. Figure 3 shows the relationship between Δt and the r.m.s. value of the fluctuation of statistics normalised by its mean value among all blocks at (*a*) $x/d = 10$ and (*b*) $x/d = 40$. The r.m.s. values of the fluctuation of statistics represent the variations in the statistics among the measurements which are conducted over Δt. It is found that as Δt increases, these r.m.s. values become small. When Δt is larger than 20 s, the variations in the statistics among the measurements are almost independent of Δt, indicating convergence. Thus, the time interval 21 s, over which the time average is taken in this study, is sufficiently long to obtain converged statistics. Even if the time averages are taken over a longer time interval than 21 s, the variations in the statistics among the measurements do not become zero. These variations are treated as the error arising from uncertainty of the measurement. To quantify this error, the results in figure 3 for $\Delta t = 21$ s are summarised in table 1. It is found that the errors are approximately 2–7 % for the mean concentrations and the mean axial velocity and approximately 5–12 % for the turbulent mass fluxes.

4. Results and discussion

Figure 4 shows the mean concentrations $\langle \Gamma_\alpha\rangle$ of species α ($\alpha = $ A, B or R) on the jet centreline for $Da = 11.8$, compared with the mean concentrations for the frozen and

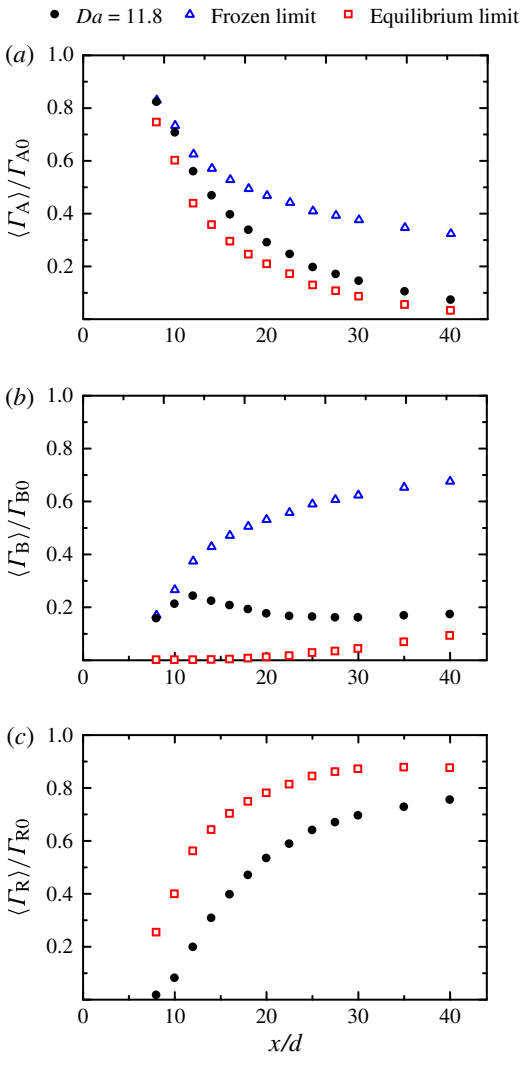

FIGURE 4. (Colour online) Mean concentration of (*a*) reactant A, (*b*) reactant B and (*c*) product R, on the jet centreline.

	$\langle \Gamma_C \rangle$ (%)	$\langle \Gamma_R \rangle$ (%)	$\langle U \rangle$ (%)	$\langle u\gamma_C \rangle$ (%)	$\langle u\gamma_R \rangle$ (%)
$x/d = 10$:	1.7	2.0	2.7	4.8	6.2
$x/d = 40$:	7.2	7.0	4.3	12.0	11.8

TABLE 1. The errors in the statistics arising from uncertainty of the measurement.

equilibrium limits. The mean concentrations of reactants A and B decrease owing to the chemical reaction. The decrease in $\langle \Gamma_A \rangle$ and $\langle \Gamma_B \rangle$ due to the chemical reaction for the equilibrium limit is larger than that for $Da = 11.8$. The mean concentration of product R increases in the axial direction because of the progress of the chemical reaction. The mean concentration of product R for the equilibrium limit is larger than

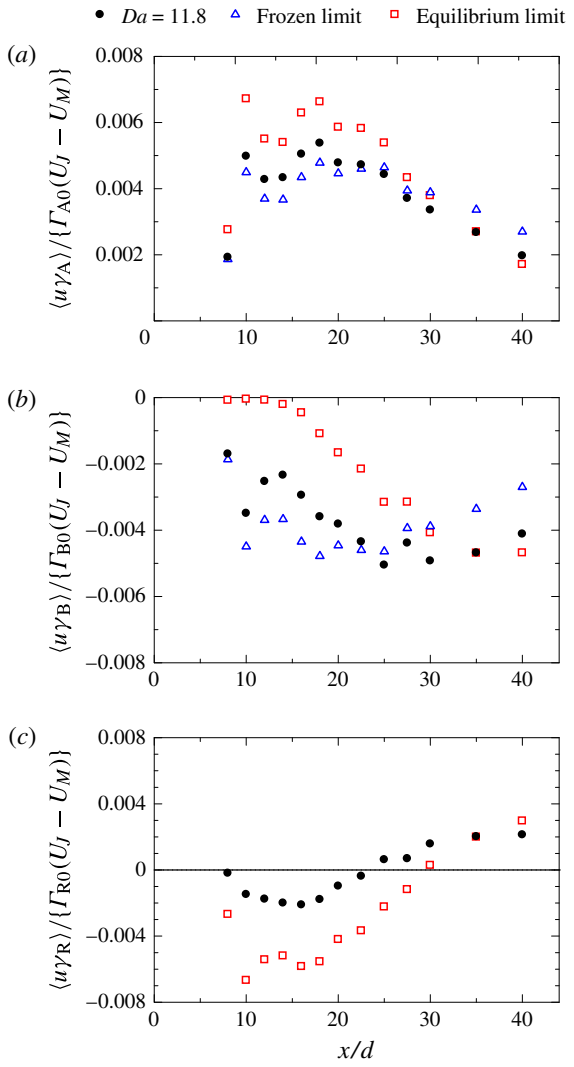

FIGURE 5. (Colour online) Turbulent mass flux of (*a*) reactant A, (*b*) reactant B and (*c*) product R, on the jet centreline.

that for $Da = 11.8$. Figure 5 shows the axial turbulent mass flux $\langle u\gamma_\alpha \rangle$ of species α ($\alpha = $ A, B or R) on the jet centreline. Comparison of $\langle u\gamma_A \rangle$ between the frozen limit and the reactive flows ($Da = 11.8$ and the equilibrium limit) shows that the chemical reaction makes $\langle u\gamma_A \rangle$ large in the upstream region but small in the downstream region. In contrast, for reactant B, the chemical reaction makes $\langle u\gamma_B \rangle$ small in magnitude in the upstream region but large in the downstream region. For product R, $\langle u\gamma_R \rangle$ is negative in the upstream region but is positive in the downstream region. These effects of chemical reaction on $\langle \Gamma_\alpha \rangle$ and $\langle u\gamma_\alpha \rangle$ have been thoroughly discussed in Watanabe *et al.* (2012).

Figure 6 shows $\partial \langle \Gamma_\alpha \rangle / \partial x$ on the jet centreline, again for $Da = 11.8$ and the frozen and equilibrium limits. Here $\langle \Gamma_\alpha \rangle$ and x are normalised by $\Gamma_{\alpha 0}$ and d, respectively. Figure 6(*a*) shows that $\partial \langle \Gamma_A \rangle / \partial x$ is negative, and the chemical reaction makes

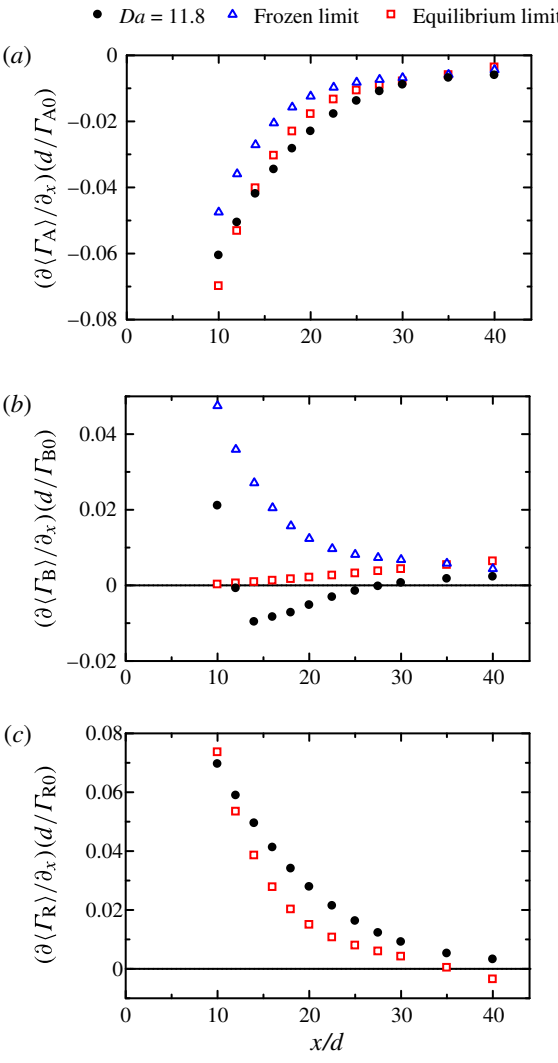

FIGURE 6. (Colour online) Axial gradient of mean concentration of (*a*) reactant A, (*b*) reactant B and (*c*) product R, on the jet centreline.

$\partial\langle\Gamma_A\rangle/\partial x$ large in magnitude because $\langle\Gamma_A\rangle$ decreases in the downstream direction as a result of consumption by the chemical reaction as well as diffusion of reactant A. Figure 6(*b*) shows that $\partial\langle\Gamma_B\rangle/\partial x$ in the reactive flow differs significantly from that for the frozen limit. In the region of $x/d < 12$, $\partial\langle\Gamma_B\rangle/\partial x$ is positive because the chemical reaction rate is small and the mean concentration of reactant B increases on the jet centreline because of entrainment. It should be noted that (3.6) for the frozen limit is written as $\Gamma_A^0/\Gamma_{A0} + \Gamma_B^0/\Gamma_{B0} = 1$, namely, $\partial(\langle\Gamma_A^0\rangle/\Gamma_{A0})/\partial x = -\partial(\langle\Gamma_B^0\rangle/\Gamma_{B0})/\partial x$. In the region $12 \leqslant x/d \leqslant 27.5$, the chemical reaction rate is large, and $\langle\Gamma_B\rangle$ decreases in the downstream direction because the chemical reaction consumes reactant B. Then, $\partial\langle\Gamma_B\rangle/\partial x$ becomes negative in the region $12 \leqslant x/d \leqslant 27.5$. Further downstream, the chemical reaction rate is small because most of A has reacted. Therefore, $\langle\Gamma_B\rangle$ increases in the downstream direction because of entrainment, resulting in

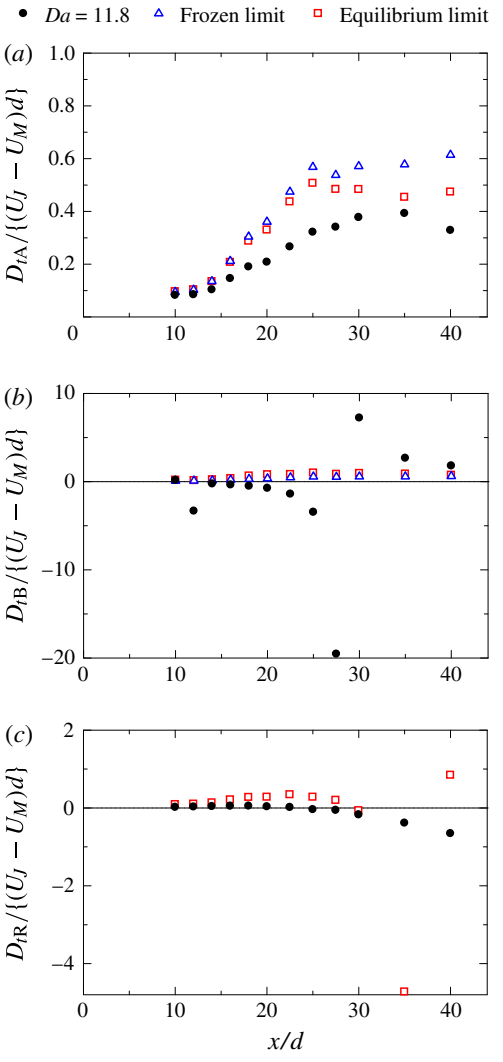

FIGURE 7. (Colour online) Eddy diffusivity of (*a*) reactant A, (*b*) reactant B and (*c*) product R, on the jet centreline.

positive $\partial\langle\Gamma_B\rangle/\partial x$. Figure 6(*c*) shows that $\partial\langle\Gamma_R\rangle/\partial x$ is large in the upstream region and decreases in the downstream direction because of the reduction of the chemical reaction rate. For the equilibrium limit, $\partial\langle\Gamma_R^{\infty}\rangle/\partial x$ becomes negative in the region $x/d > 35$ because the production of R is smaller than the decrement arising from the diffusion of R.

The eddy diffusivity $D_{t\alpha}$ is estimated from $D_{t\alpha} = \langle u\gamma_\alpha\rangle/(-\partial\langle\Gamma_\alpha\rangle/\partial x)$. It is shown in figure 7 for species α = A, B or R on the jet centreline. Because D_{tB} and D_{tR} change greatly owing to the chemical reaction, figures 7(*b*) and 7(*c*) are enlarged in figure 8 to investigate D_{tB} and D_{tR} in detail. In figures 7 and 8, the eddy diffusivities for the frozen and equilibrium limits are also shown, and $D_{t\alpha}$ is normalized by d and $(U_J - U_M)$. Figure 7(*a*) shows that the chemical reaction makes D_{tA} small and D_{tB} (figure 7*b*) for the frozen limit is positive in the entire region on the

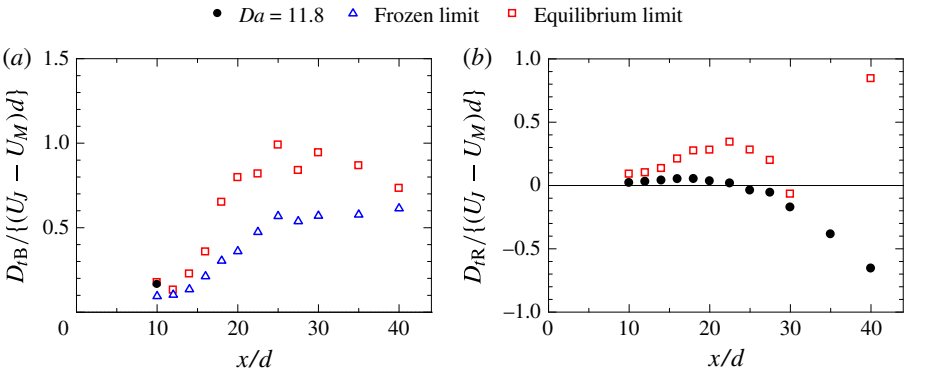

FIGURE 8. (Colour online) Eddy diffusivity of (*a*) reactant B and (*b*) product R on the jet centreline.

jet centreline. Figures 6(*b*), 7(*b*) and 8(*a*) show that D_{tB} is positive in the region where $\partial\langle\Gamma_B\rangle/\partial x > 0$. However, in the region where $\partial\langle\Gamma_B\rangle/\partial x < 0$, D_{tB} is negative and counter-gradient diffusion is observed. D_{tB} discontinuously varies on the jet centreline because $\partial\langle\Gamma_B\rangle/\partial x$ can be zero: at this location, the eddy diffusivity expression for the axial turbulent mass flux is ill-defined. For the frozen limit, $\partial(\langle\Gamma_A^0\rangle/\Gamma_{A0})/\partial x = -\partial(\langle\Gamma_B^0\rangle/\Gamma_{B0})/\partial x$ and $\langle u\gamma_A^0\rangle/\Gamma_{A0} = -\langle u\gamma_B^0\rangle/\Gamma_{B0}$. Hence, D_{tA} is identical to D_{tB} in the non-reactive flow. This relationship can be confirmed in figures 7(*a*) and 8(*a*). Figures 7(*c*) and 8(*b*) show that D_{tR} is positive in the region $x/d < 25$ but is negative in the region $x/d \geqslant 25$. Here D_{tR} for the equilibrium limit discontinuously varies because $\partial\langle\Gamma_R\rangle/\partial x$ becomes zero at $x/d \simeq 35$ as shown in figure 6(*c*). The eddy diffusivity of the reactive species is different for $Da = 11.8$ and the equilibrium limit. Thus, the effects of chemical reaction on the eddy diffusivity depend on the Damköhler number.

A large difference in the eddy diffusivity can be observed between reactants A and B, which are supplied from the jet and ambient flows, respectively. Here, we separately consider the transport of the reactants by the velocity field and the effect of the reaction on the concentrations of the reactants. First, we consider the former. The concentration of reactant A on the jet centreline decreases in the axial direction because of diffusion, whereas the concentration of reactant B on the jet centreline increases in the axial direction because it is entrained from the ambient flow. Thus, the transport by the velocity field has an opposite effect on the concentration on the jet centreline for reactants A and B. In contrast, the chemical reaction simply decreases the concentrations of both reactants A and B. The concentration of reactant B in the jet increases by entrainment but decreases by chemical reaction. Therefore, the mean concentration profile of reactant B on the jet centreline is significantly different for the reactive and non-reactive cases, and the axial gradient of its concentration can be both positive and negative. The concentration of reactant A in the jet decreases owing to both diffusion and chemical reaction, and its mean concentration monotonically decreases in the axial direction on the jet centreline. The change in the sign of the mean concentration gradient due to the chemical reaction is important in considering the gradient diffusion model in the reactive planar jet. Therefore, it is expected to be crucial for the gradient diffusion model whether the reactant is supplied from the jet or the ambient flow.

The eddy diffusivity of reactant species measured in the scalar mixing layer in liquid (Komori *et al.* 1993) is larger than that of non-reactive species. However, Bilger *et al.* (1991) show that in the scalar mixing layer in gas, the chemical reaction makes the eddy diffusivity of reactant species large in the region where the reactant is abundant but small in the region where the reactant is deficient. Additionally, the eddy diffusivity measured by Bilger *et al.* (1991) and Komori *et al.* (1993) is always positive, and counter-gradient diffusion was not observed. In contrast, in this study, the eddy diffusivity of reactant B premixed into the ambient flow can be negative, and counter-gradient diffusion is observed. The effects of the chemical reaction on the eddy diffusivity observed in our study and in those of Bilger *et al.* (1991) and Komori *et al.* (1993) are different from each other. This difference implies that the effects of the chemical reaction on the eddy diffusivity can change with the flow field, the molecular Schmidt number and the Damköler number, although the present results are not enough to specify the factors which can affect the gradient diffusion model for reactive flows.

The transport equation for the turbulent mass flux of reactive species α (Fox 2003) can be written as follows:

$$\frac{\partial \langle u_i \gamma_\alpha \rangle}{\partial t} + \langle U_j \rangle \frac{\partial \langle u_i \gamma_\alpha \rangle}{\partial x_j} = \frac{\partial}{\partial x_j} \left(T_{ij\alpha} - \langle u_j u_i \gamma_\alpha \rangle \right) + P_{i\alpha} + \Pi_{i\alpha} - \epsilon_{i\alpha} + \langle u_i s_\alpha \rangle, \tag{4.1}$$

where $s_\alpha = S_\alpha - \langle S_\alpha \rangle$ is the fluctuating component of the chemical reaction rate. The molecular-transport term $T_{ij\alpha}$, the pressure-scrambling term $\Pi_{i\alpha}$ and the scalar-flux dissipation $\epsilon_{i\alpha}$ are expressed as

$$T_{ij\alpha} \equiv \nu \left\langle \gamma_\alpha \frac{\partial u_i}{\partial x_j} \right\rangle + D_\alpha \left\langle u_i \frac{\partial \gamma_\alpha}{\partial x_j} \right\rangle, \tag{4.2}$$

$$\Pi_{i\alpha} \equiv - \left\langle \gamma_\alpha \frac{\partial p}{\partial x_i} \right\rangle, \tag{4.3}$$

$$\epsilon_{i\alpha} \equiv (\nu + D_\alpha) \left\langle \frac{\partial u_i}{\partial x_j} \frac{\partial \gamma_\alpha}{\partial x_j} \right\rangle. \tag{4.4}$$

Here, p is the pressure fluctuation. The production term $P_{i\alpha}$ is expressed as

$$P_{i\alpha} \equiv P_{i\alpha 1} + P_{i\alpha 2}, \tag{4.5}$$

$$P_{i\alpha 1} \equiv -\langle u_i u_j \rangle \frac{\partial \langle \Gamma_\alpha \rangle}{\partial x_j}, \tag{4.6}$$

$$P_{i\alpha 2} \equiv -\langle u_j \gamma_\alpha \rangle \frac{\partial \langle U_i \rangle}{\partial x_j}. \tag{4.7}$$

First, we investigate the direct influence on the turbulent mass flux budget of the chemical reaction, which is represented by $\langle u s_\alpha \rangle$ for the axial turbulent mass flux of concentration of species α. Here $\langle u s_\alpha \rangle$ can be also represented by $\langle u S_\alpha \rangle$ because $\langle u S_\alpha \rangle = \langle u \rangle \langle S_\alpha \rangle + \langle u s_\alpha \rangle = \langle u s_\alpha \rangle$. For the chemical reaction $\mathrm{A} + \mathrm{B} \rightarrow \mathrm{R}$, the chemical source term is given by $S_\mathrm{R} = -S_\mathrm{A} = -S_\mathrm{B} = k \Gamma_\mathrm{A} \Gamma_\mathrm{B}$. For the frozen limit, $\langle u S_\alpha \rangle$ is zero because the frozen limit corresponds to the non-reactive case ($k = 0$). For the equilibrium limit, either of the instantaneous concentrations of reactants A or B is zero as shown in (3.10) and (3.11). Therefore, $\langle u S_\alpha \rangle$ is also zero for the equilibrium limit. Here, we compare $\langle u \Gamma_\mathrm{A} \Gamma_\mathrm{B} \rangle$ instead of $\langle u S_\mathrm{R} \rangle = k \langle u \Gamma_\mathrm{A} \Gamma_\mathrm{B} \rangle$ between the reactive

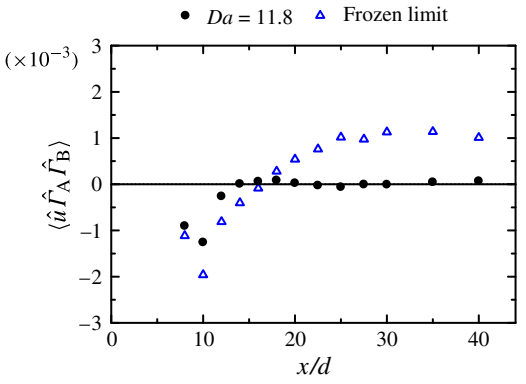

FIGURE 9. (Colour online) $\langle \hat{u}\hat{\Gamma}_A\hat{\Gamma}_B\rangle$ on the jet centreline; $\langle \hat{u}\hat{\Gamma}_A\hat{\Gamma}_B\rangle$ is related to the direct influence on the turbulent mass flux budget of the chemical reaction.

flow ($Da = 11.8$) and the non-reactive flow (the frozen limit), because $\langle u\Gamma_A\Gamma_B\rangle$ can be calculated for both the frozen limit and the reactive case with a finite reaction rate. Figure 9 shows $\langle \hat{u}\hat{\Gamma}_A\hat{\Gamma}_B\rangle$ on the jet centreline, where $\hat{u} = u/(U_J - U_M)$ and $\hat{\Gamma}_\alpha = \Gamma_\alpha/\Gamma_{\alpha 0}$. In the upstream region, $\langle \hat{u}\hat{\Gamma}_A\hat{\Gamma}_B\rangle$ is negative for both reactive and non-reactive cases. In the non-reactive flow, $\langle \hat{u}\hat{\Gamma}_A\hat{\Gamma}_B\rangle$ increases in the downstream direction and becomes positive. On the other hand, $\langle \hat{u}\hat{\Gamma}_A\hat{\Gamma}_B\rangle$ in the reactive flow is small in magnitude in the downstream region. These profiles can be explained as follows: by using (3.4) and (3.5), the product of the normalized concentrations of reactants A and B can be written as follows:

$$\hat{\Gamma}_A\hat{\Gamma}_B = \hat{\Gamma}_A(1-\hat{\Gamma}_R-\hat{\Gamma}_A) = -\left\{\hat{\Gamma}_A - \tfrac{1}{2}(1-\hat{\Gamma}_R)\right\}^2 + \tfrac{1}{4}(1-\hat{\Gamma}_R)^2 \tag{4.8}$$

$$= \hat{\Gamma}_B(1-\hat{\Gamma}_R-\hat{\Gamma}_B) = -\left\{\hat{\Gamma}_B - \tfrac{1}{2}(1-\hat{\Gamma}_R)\right\}^2 + \tfrac{1}{4}(1-\hat{\Gamma}_R)^2. \tag{4.9}$$

Thus, $\hat{\Gamma}_A\hat{\Gamma}_B$ is a quadratic function of $\hat{\Gamma}_A$ (and $\hat{\Gamma}_B$). Equations (4.8) and (4.9) imply that $\hat{\Gamma}_A\hat{\Gamma}_B$ becomes maximum for the condition $\hat{\Gamma}_A = \hat{\Gamma}_B = (1-\hat{\Gamma}_R)/2$. Further discussion on the relationship between the reaction rate ($k\hat{\Gamma}_A\hat{\Gamma}_B$) and the concentrations of the reactants can be found in Watanabe *et al.* (2012). The sign of $\langle \hat{u}\hat{\Gamma}_A\hat{\Gamma}_B\rangle$ is determined by the correlation between $\hat{u}$ and $\hat{\Gamma}_A\hat{\Gamma}_B$. In the upstream region on the jet centreline, the reactant B is deficient (figure 4), and $\hat{\Gamma}_B$ tends to be smaller than $\hat{\Gamma}_A$. Because $\hat{\Gamma}_A\hat{\Gamma}_B$ becomes maximum for the condition $\hat{\Gamma}_A = \hat{\Gamma}_B$, the large $\hat{\Gamma}_A\hat{\Gamma}_B$ in the upstream region on the jet centreline can be related to the large concentration of reactant B. The turbulent mass flux $\langle \hat{u}\hat{\gamma}_\alpha\rangle$ can be represented by $\langle \hat{u}\hat{\gamma}_\alpha\rangle = \langle \hat{u}\rangle\langle \hat{\Gamma}_\alpha\rangle + \langle \hat{u}\hat{\gamma}_\alpha\rangle = \langle \hat{u}\hat{\Gamma}_\alpha\rangle$. Because of the negative correlation between $\hat{u}$ and $\hat{\Gamma}_B$ (figure 5*b*), when $\hat{u}$ is negative, $\hat{\Gamma}_B$ tends to be large, resulting in the large $\hat{\Gamma}_A\hat{\Gamma}_B$. Therefore, because $\hat{\Gamma}_A\hat{\Gamma}_B$ is always positive, $\langle \hat{u}\hat{\Gamma}_A\hat{\Gamma}_B\rangle$ is negative in the upstream region. In contrast, reactant A is deficient in the downstream region as shown in figure 4, and $\hat{\Gamma}_A$ tends to be smaller than $\hat{\Gamma}_B$. Because $\hat{\Gamma}_A\hat{\Gamma}_B$ becomes maximum for the condition $\hat{\Gamma}_A = \hat{\Gamma}_B$, the large $\hat{\Gamma}_A\hat{\Gamma}_B$ in the downstream region can be related to the large concentration of reactant A. Because of positive correlation between $\hat{u}$ and $\hat{\Gamma}_A$ (figure 5*a*), when $\hat{u}$ is positive, $\hat{\Gamma}_A$ tends to be large, resulting in the large $\hat{\Gamma}_A\hat{\Gamma}_B$.

Therefore, $\langle \hat{u}\hat{\Gamma}_{\mathrm{A}}\hat{\Gamma}_{\mathrm{B}}\rangle$ is positive in the downstream region. In the reactive case, because the concentration of reactant A becomes small as shown in figure 4(*a*) because of the chemical consumption, $\hat{\Gamma}_{\mathrm{A}}\hat{\Gamma}_{\mathrm{B}}$ is small in the downstream region. Therefore, in the reactive flow, $\langle \hat{u}\hat{\Gamma}_{\mathrm{A}}\hat{\Gamma}_{\mathrm{B}}\rangle$ becomes small in the downstream region.

Thus, it is found that the chemical reaction term $\langle us_{\alpha}\rangle$ directly affects the turbulent mass flux budget in the upstream region where the chemical reaction rate is not small. Although the direct influence of the chemical reaction is important in the upstream region, the turbulent mass flux changes owing to the chemical reaction even in the downstream region as shown in figure 5. Therefore, not only the chemical reaction term $\langle us_{\alpha}\rangle$ but also the other terms such as the production term are responsible for the change in the turbulent mass flux by the chemical reaction.

Next, we consider the change in the production term $P_{x\alpha}$ due to the chemical reaction to investigate the effect of the chemical reaction on the eddy diffusivity. Statistics in the planar jet are symmetrical with respect to the x-axis ($y = 0$) and homogeneous in the spanwise direction. Therefore, the lateral and spanwise components of the production term are zero on the jet centreline, and the production term is determined solely by the axial component. Although the spanwise component does not exist in the entire region of the planar jet, the lateral component contributes to the production term in the planar jet except for the jet centreline. On the jet centreline, $P_{x\alpha 1}$ and $P_{x\alpha 2}$ are given by

$$P_{x\alpha 1} = -\langle u^2\rangle \frac{\partial \langle \Gamma_{\alpha}\rangle}{\partial x}, \tag{4.10}$$

$$P_{x\alpha 2} = -\langle u\gamma_{\alpha}\rangle \frac{\partial \langle U\rangle}{\partial x}. \tag{4.11}$$

Figure 10 shows $\hat{P}_{x\alpha 1} \equiv P_{x\alpha 1}d/\{(U_J - U_M)^2\Gamma_{\alpha 0}\}$ on the jet centreline. Because the chemical reaction is passive with respect to the flow field, the change in $\hat{P}_{i\alpha 1}$ due to the chemical reaction corresponds to the change in the mean concentration gradient. The axial gradient of the mean concentration of reactant A, which is always negative on the jet centreline, becomes large in magnitude owing to the chemical reaction (see figure 6*a*). Hence, the chemical reaction increases $\hat{P}_{x\mathrm{A}1}$. Here $\hat{P}_{x\mathrm{B}1}$ for the frozen limit is negative on the jet centreline because $\partial\langle\Gamma_{\mathrm{B}}\rangle/\partial x$ is always positive (see figure 6*b*). However, $\hat{P}_{x\mathrm{B}1}$ for $Da = 11.8$ can be positive because the chemical reaction changes the sign of $\partial\langle\Gamma_{\mathrm{B}}\rangle/\partial x$, as shown in figure 6(*b*). Here $\hat{P}_{x\mathrm{B}1}$ for the equilibrium limit is very small; however, its sign does not change owing to the chemical reaction. In the region $x/d > 10$, $\hat{P}_{x\mathrm{R}1}$ becomes small in magnitude in the axial direction. Here $\hat{P}_{x\mathrm{R}1}$ for the equilibrium limit becomes positive in the downstream region because of the negative value of $\partial\langle\Gamma_{\mathrm{R}}\rangle/\partial x$ (figure 6*c*).

Figure 11 shows $\hat{P}_{x\alpha 2} \equiv P_{x\alpha 2}d/\{(U_J - U_M)^2\Gamma_{\alpha 0}\}$ on the jet centreline. The change in $\hat{P}_{x\alpha 2}$ due to the chemical reaction corresponds to the change in the turbulent mass flux. The chemical reaction makes $\hat{P}_{x\mathrm{A}2}$ large in the upstream region but slightly smaller in the downstream region. In contrast, the chemical reaction makes $\hat{P}_{x\mathrm{B}2}$ small in magnitude in the upstream region but large in the downstream region. The sign of $\hat{P}_{x\mathrm{B}2}$ does not change owing to the chemical reaction, whereas the sign of $\hat{P}_{x\mathrm{B}1}$ depends on the axial gradient of $\langle\Gamma_{\mathrm{B}}\rangle$ as shown in figure 10(*b*). Figure 11(*c*) shows that $\hat{P}_{x\mathrm{R}2}$ is negative in the upstream region and becomes positive in the downstream region.

Figure 12 shows the normalised production term $\hat{P}_{x\alpha} \equiv \hat{P}_{x\alpha 1} + \hat{P}_{x\alpha 2}$ on the jet centreline. Comparison between $\hat{P}_{x\mathrm{A}1}$ (figure 10*a*) and $\hat{P}_{x\mathrm{A}2}$ (figure 11*a*) shows that

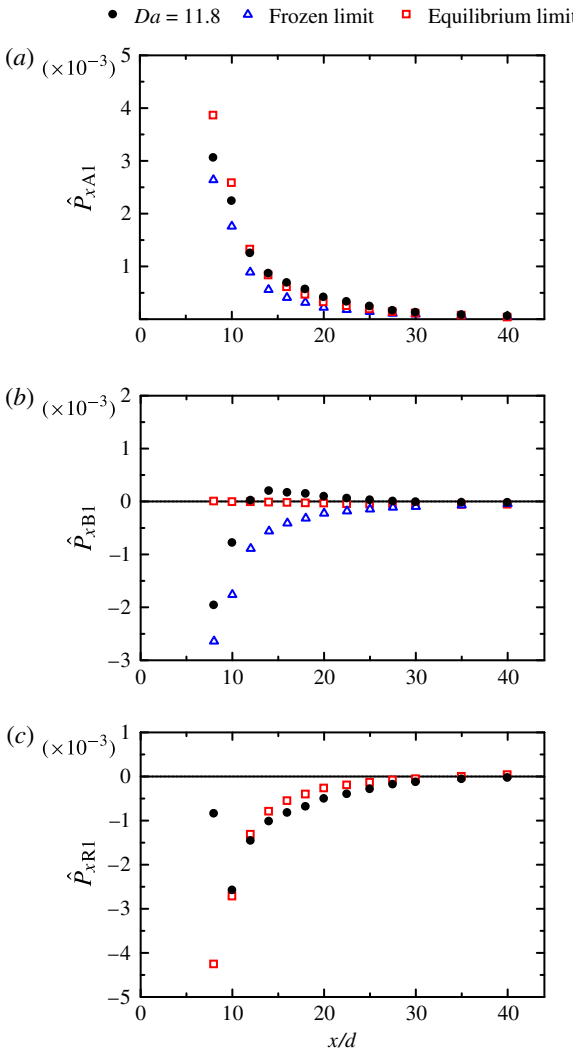

FIGURE 10. (Colour online) $P_{x\alpha 1}$ given by (4.10) on the jet centreline for (*a*) reactant A, (*b*) reactant B and (*c*) product R.

$\hat{P}_{x\mathrm{A}1}$ makes a much larger contribution to $\hat{P}_{x\mathrm{A}}$. The profiles of $\hat{P}_{x\mathrm{B}}$ and $\hat{P}_{x\mathrm{R}}$ are also similar to those for $\hat{P}_{x\mathrm{B}1}$ and $\hat{P}_{x\mathrm{R}1}$. However, because $\hat{P}_{x\mathrm{B}1}$ and $\hat{P}_{x\mathrm{R}1}$ can be equal to zero as shown in figure 10(*b*,*c*), $\hat{P}_{x\mathrm{B}2}$ and $\hat{P}_{x\mathrm{R}2}$ are important in the production of turbulent mass flux. The production term $\hat{P}_{x\alpha}$ divided by $(-\partial\langle\hat{\Gamma}_\alpha\rangle/\partial\hat{x})$ is shown in figure 13 to investigate the relationship between the axial gradients of the mean concentrations and the production of the axial turbulent mass fluxes. Here, $\hat{x} \equiv x/d$. For reactant A, the chemical reaction hardly changes $\hat{P}_{x\mathrm{A}}/(-\partial\langle\hat{\Gamma}_\mathrm{A}\rangle/\partial\hat{x})$. For reactant B, $\hat{P}_{x\mathrm{B}}/(-\partial\langle\hat{\Gamma}_\mathrm{B}\rangle/\partial\hat{x})$ changes significantly owing to the chemical reaction and can be negative for $Da = 11.8$. It should be noted that from (4.10) and (4.11), when the magnitude of $P_{x\alpha 2}$ is much smaller than that of $P_{x\alpha 1}$, $P_{x\alpha}/(-\partial\langle\Gamma_\alpha\rangle/\partial x) \approx \langle u^2\rangle > 0$ on the jet centreline, and $P_{x\alpha}/(-\partial\langle\Gamma_\alpha\rangle/\partial x)$ does not change owing to the chemical

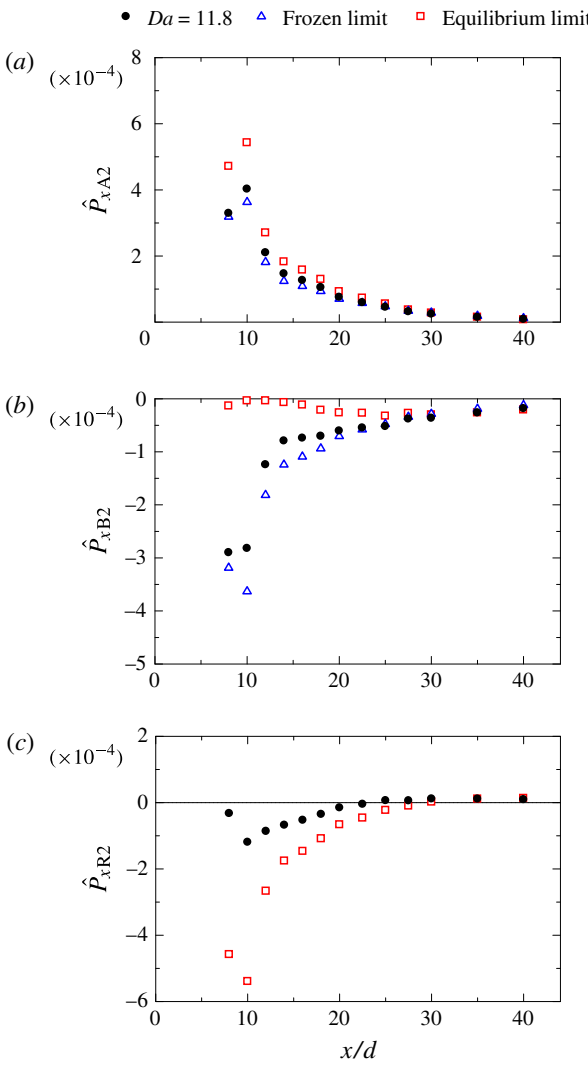

FIGURE 11. (Colour online) $P_{x\alpha 2}$ given by (4.11) on the jet centreline for (*a*) reactant A, (*b*) reactant B and (*c*) product R.

reaction. Thus, the negative values of $\hat{P}_{x\mathrm{B}}/(-\partial\langle\hat{\Gamma}_{\mathrm{B}}\rangle/\partial\hat{x})$ arise from the large contribution of $\hat{P}_{x\mathrm{B}2}$ to $\hat{P}_{x\mathrm{B}}$ in the region where $\hat{P}_{x\mathrm{B}1} \approx 0$. Considering (1.2), one sees that this difference of sign between $\hat{P}_{x\mathrm{B}}$ and $(-\partial\langle\hat{\Gamma}_{\mathrm{B}}\rangle/\partial\hat{x})$ is assumed to cause the counter-gradient flux of reactant B. Figure 13(*c*) shows that $\hat{P}_{x\mathrm{R}}$ divided by $(-\partial\langle\hat{\Gamma}_{\mathrm{R}}\rangle/\partial\hat{x})$ also can be negative for the equilibrium limit. For reactant B and product R, the production term can produce an axial turbulent mass flux opposite to the axial gradient direction of the mean concentrations on the jet centreline. The region where $\hat{P}_{x\alpha}/(-\partial\langle\hat{\Gamma}_{\alpha}\rangle/\partial\hat{x})$ ($\alpha = \mathrm{B}$ or R) is negative does not entirely match the region where the eddy diffusivity is negative because the change in the turbulent mass flux due to the chemical reaction is not determined solely by the production term. The production term, however, significantly affects the profile of the turbulent mass

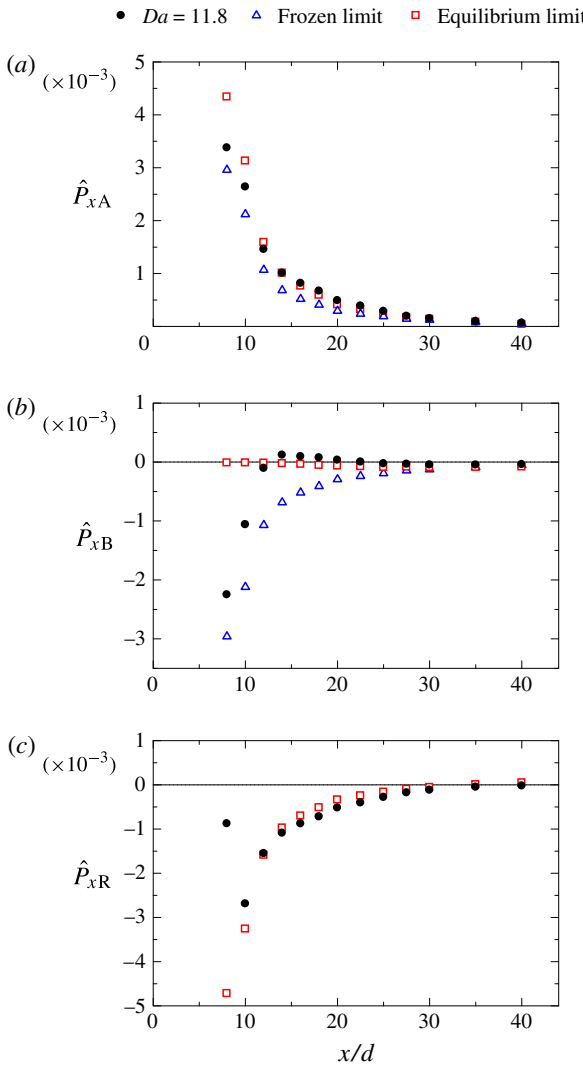

FIGURE 12. (Colour online) Production term of axial turbulent mass flux on the jet centreline for (*a*) reactant A, (*b*) reactant B and (*c*) product R.

flux. These changes of the production term result in the negative eddy diffusivity of reactant B and product R.

Figure 14 compares the chemical source terms and the production terms for $Da = 11.8$. For the transport equation normalized by $(U_J - U_M)$ and $\Gamma_{\alpha 0}$, the chemical source terms for A, B and R are represented by $-Da\xi_S\langle\hat{u}\hat{\Gamma}_\mathrm{A}\hat{\Gamma}_\mathrm{B}\rangle$, $-Da(1-\xi_S)\langle\hat{u}\hat{\Gamma}_\mathrm{A}\hat{\Gamma}_\mathrm{B}\rangle$ and $Da\langle\hat{u}\hat{\Gamma}_\mathrm{A}\hat{\Gamma}_\mathrm{B}\rangle$, respectively. Because the chemical source terms are calculated from triple correlations, it is difficult to obtain their profiles which are converged as well as the production terms. However, it is clearly seen that the chemical source terms are important at $x/d = 10$ compared with the production terms because of the large reaction rate in this region.

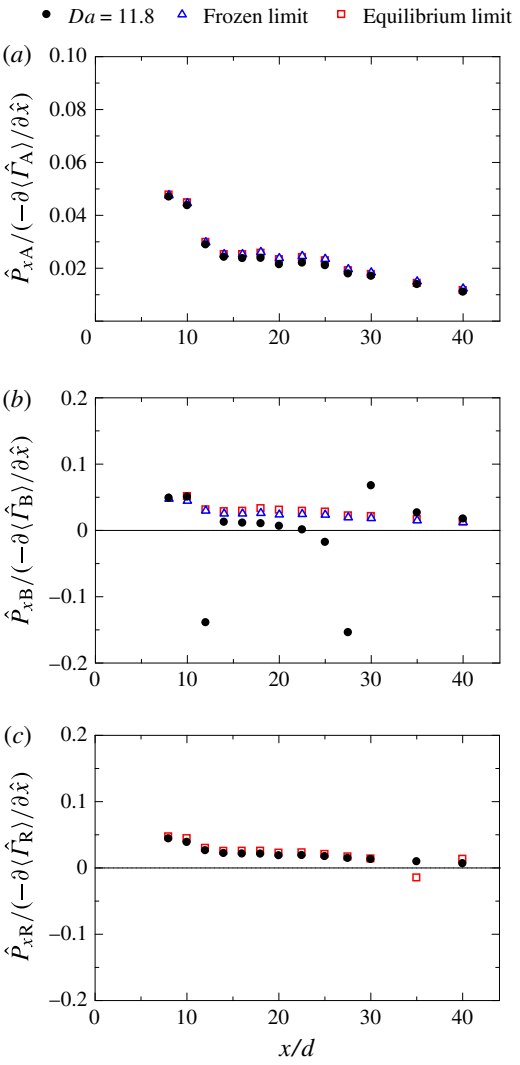

FIGURE 13. (Colour online) Comparison between the axial gradient of mean concentration and the production term of axial turbulent mass flux for (*a*) reactant A, (*b*) reactant B and (*c*) product R.

In the eddy viscosity model (Combest *et al.* 2011), the Reynolds stress is given by

$$-\langle u_i u_j \rangle = \nu_t \left(\frac{\partial \langle U_i \rangle}{\partial x_j} + \frac{\partial \langle U_j \rangle}{\partial x_i} \right) - \frac{2}{3} \delta_{ij} k_t, \tag{4.12}$$

where $k_t = \langle u_k u_k \rangle / 2$ is a turbulent kinetic energy, δ_{ij} is the Kronecker delta and ν_t is the eddy viscosity. In the self-preserving region of the planar jet, ν_t can be written as (Pope 2000)

$$\nu_t(x, y) = \left[\ln(1 + \sqrt{2})^2 \right]^{-2} \frac{\mathrm{d}b_U}{\mathrm{d}x} U_C(x) b_U(x), \tag{4.13}$$

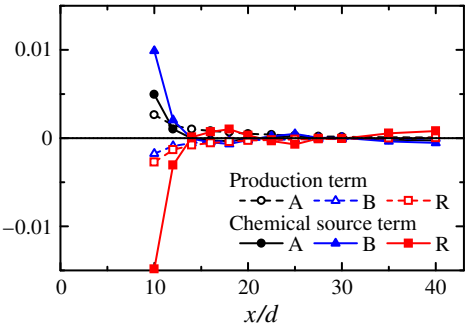

FIGURE 14. (Colour online) Comparison between the chemical source terms and the production terms for $Da = 11.8$. These terms are normalized by $U_J - U_M$ and $\Gamma_{\alpha 0}$.

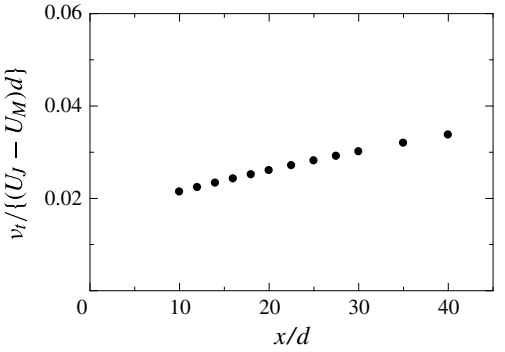

FIGURE 15. Eddy viscosity on the jet centreline.

where $U_C(x)$ is the mean axial velocity difference on the jet centreline, $(\langle U\rangle - U_M)_{y=0}$, and $b_U(x)$ is the jet half-width of the mean axial velocity difference $(\langle U\rangle - U_M)$. Figure 15 shows the axial profile of normalised ν_t calculated from (4.13) in the self-preserving region. In the self-preserving region of the planar jet, $U_C \propto (x/d)^{-1/2}$ and $b_U \propto x/d$, and then ν_t is proportional to $(x/d)^{1/2}$ in the x direction.

The turbulent Schmidt number $Sc_{t\alpha}$ ($\alpha = $ A, B or R) on the jet centreline is shown in figure 16, and the frozen and equilibrium limits are also shown. Figure 16(*a*) shows that the chemical reaction makes $Sc_{t\mathrm{A}}$ large. However, $Sc_{t\mathrm{A}}$ for the equilibrium limit is close to $Sc_{t\mathrm{A}}$ for the frozen limit. This implies that the effect of chemical reaction on $Sc_{t\mathrm{A}}$ depends on the Damköhler number. In figure 16(*b*), it is shown that $Sc_{t\mathrm{B}}$ becomes small owing to the chemical reaction. In the region $12 \leqslant x/d \leqslant 27.5$, $Sc_{t\mathrm{B}}$ for $Da = 11.8$ is negative because $D_{t\mathrm{B}} < 0$ in this region. Here $Sc_{t\mathrm{B}}$ in the reactive flow approaches the values for the frozen limit in the downstream direction. Figure 16(*c*) shows that $Sc_{t\mathrm{R}}$ for $Da = 11.8$ is positive in the region of $x/d < 25$ but is negative in the region $x/d \geqslant 25$. It is also shown that $Sc_{t\mathrm{R}}$ discontinuously varies at the point where $\langle u\gamma_{\mathrm{R}}\rangle = 0$ (i.e. $D_{t\mathrm{R}} = 0$). In the region $x/d < 25$, $Sc_{t\mathrm{R}}$ for the equilibrium limit is smaller than $Sc_{t\mathrm{R}}$ for the finite Damköhler number. Therefore, it is suggested that $Sc_{t\mathrm{R}}$ becomes small in this region if the Damköhler number is large. These changes in $Sc_{t\alpha}$ due to the chemical reaction correspond to the changes in the eddy diffusivity because the chemical reaction is passive with respect to the flow field and does not affect the eddy viscosity ν_t.

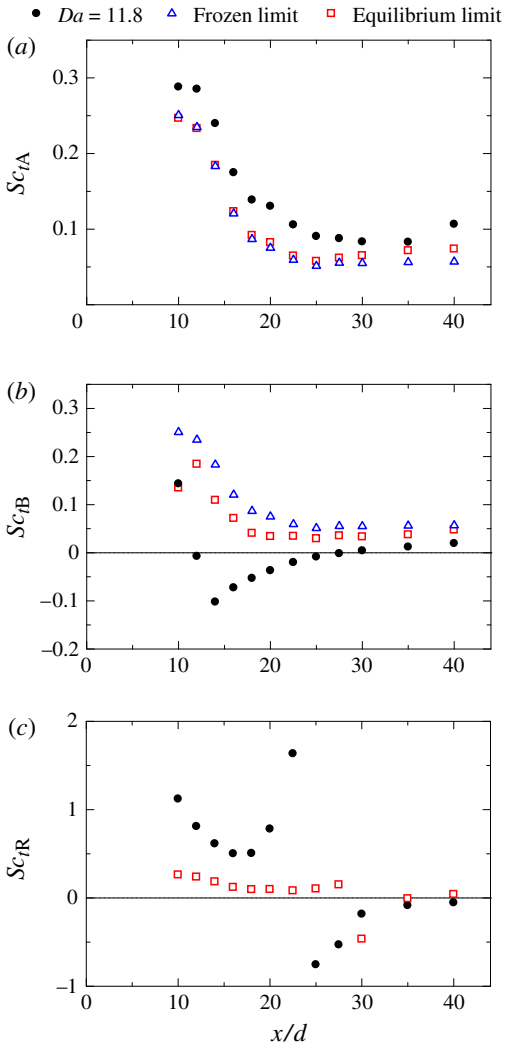

FIGURE 16. (Colour online) Turbulent Schmidt number of (*a*) reactant A, (*b*) reactant B and (*c*) product R on the jet centreline.

$Sc_{t\mathrm{B}}$ in the reactive flow is close to $Sc_{t\mathrm{B}}$ in the non-reactive flow in the far-downstream region whereas the chemical reaction greatly affects $Sc_{t\mathrm{B}}$ in the upstream region. The chemical reaction rate is small in the far-downstream region because most of A has reacted. After this, the instantaneous concentration of the other reactant B mainly changes because of convective transport and molecular diffusion. Therefore, $Sc_{t\mathrm{B}}$ for $Da = 11.8$ in the far-downstream region is nearly equal to that in the non-reactive flow. In contrast, $Sc_{t\mathrm{B}}$ in the reactive flow is very different from that in the non-reactive flow in the upstream region because the chemical reaction rate is large and the chemical reaction affects $Sc_{t\mathrm{B}}$.

In this study, it is clarified that $Sc_{t\alpha}$ for a finite Damköhler number is different from $Sc_{t\alpha}$ for the equilibrium limit. The change in $Sc_{t\alpha}$ for reactants A and B due to the chemical reaction for the equilibrium limit is smaller than that for $Da = 11.8$. $Sc_{t\alpha}$ for

the reactant species is expected to be greatly affected by the chemical reaction when the Damköhler number is small. In general, $Sc_{t\alpha}$ is assumed to be a global constant parameter. However, there is large difference in $Sc_{t\alpha}$ between reactive and non-reactive flows, as shown in figure 16.

5. Conclusion

Eddy diffusivity and turbulent Schmidt number are experimentally investigated in a planar liquid jet with a second-order chemical reaction (A + B → R). Reactant A is premixed into the jet flow and the other reactant B is premixed into the ambient flow. The eddy diffusivity $D_{t\alpha}$ and the turbulent Schmidt number $Sc_{t\alpha}$ are obtained from the measurement results of mean concentration $\langle \Gamma_\alpha \rangle$ and turbulent mass flux $\langle u\gamma_\alpha \rangle$ ($\alpha = $ A, B or R).

The chemical reaction makes $D_{t\mathrm{A}}$ small. In the reactive flow $D_{t\mathrm{B}}$ is negative in the region where $\langle \Gamma_\mathrm{B} \rangle$ decreases in the downstream direction, and counter-gradient diffusion is observed. In contrast, in the non-reactive flow $D_{t\mathrm{B}}$ is positive in the entire region on the jet centreline. In the reactive flow $D_{t\mathrm{B}}$ discontinuously varies because $\partial \langle \Gamma_\mathrm{B} \rangle / \partial x$ can be zero on the jet centreline. Negative values of the eddy diffusivity are also found for the product R. When the chemical reaction occurs, the production terms of axial turbulent mass fluxes of reactant B and product R can produce axial turbulent mass fluxes opposite to the axial gradients of the mean concentrations. The changes in the production terms due to the chemical reaction result in negative eddy diffusivities of reactant B and product R. The effects of the chemical reaction on the eddy diffusivity observed in this study are different from the results in previous research (Bilger *et al.* 1991; Komori *et al.* 1993), and this implies that the effects of chemical reactions depend on the flow field, the molecular Schmidt number of reactive species, the Damköhler number and possibly other factors.

The chemical reaction makes $Sc_{t\mathrm{A}}$ large; $Sc_{t\mathrm{B}}$ and $Sc_{t\mathrm{R}}$ can be negative when the chemical reaction occurs. The difference in $Sc_{t\mathrm{B}}$ between the reactive and non-reactive flows becomes small in the far-downstream region. It is also found that $Sc_{t\alpha}$ for reactants A and B significantly changes owing to the chemical reaction when the Damköhler number is small.

Chemical reactions significantly affect the eddy diffusivity and the turbulent Schmidt number of reactive species. Applying the gradient diffusion model to reactive flows may result in significant errors in estimating turbulent mass fluxes under the assumption of global constant turbulent Schmidt numbers.

Acknowledgements

K.N. acknowledges Professor S. Komori (Kyoto University) for providing the main idea of this study and many valuable suggestions. The authors acknowledge the anonymous referees for valuable comments. This work was supported by JSPS KAKENHI grant number 25002531 and MEXT KAKENHI grant numbers 25289030, 25289031 and 2563005.

REFERENCES

BILGER, R. W., SAETRAN, L. R. & KRISHNAMOORTHY, L. V. 1991 Reaction in a scalar mixing layer. *J. Fluid Mech.* **233**, 211–242.

BOURNE, J. R., HILBER, C. & TOVSTIGA, G. 1985 Kinetics of the azo coupling reactions between 1-naphthol and diazotised sulphanilic acid. *Chem. Engng Commun.* **37** (1–6), 293–314.

BRAY, K. N. C., LIBBY, P. A., MASUYA, G. & MOSS, J. B. 1981 Turbulence production in premixed turbulent flames. *Combust. Sci. Technol.* **25**, 127–140.

BROWN, R. J. & BILGER, R. W. 1998*a* Experiments on a reacting plume-1. Conventional concentration statistics. *Atmos. Environ.* **32** (4), 611–628.

BROWN, R. J. & BILGER, R. W. 1998*b* Experiments on a reacting plume-2. Conditional concentration statistics. *Atmos. Environ.* **32** (4), 629–646.

DE BRUYN KOPS, S. M., RILEY, J. J. & KOSALY, G. 2001 Direct numerical simulation of reacting scalar mixing layers. *Phys. Fluids* **13**, 1450–1465.

CHAKRABORTY, N. & CANT, R. S. 2009 Effects of Lewis number on scalar transport in turbulent premixed flames. *Phys. Fluids* **21**, 035110.

CHENG, R. K. & SHEPHERD, I. G. 1991 The influence of burner geometry on premixed turbulent flame propagation. *Combust. Flame* **85**, 7–26.

CHORNYI, A. D. & ZHDANOV, V. L. 2010 Verification of chemical reaction rate models in turbulent reacting flows at Schmidt number considerably exceeding 1. *J. Engng Phys. Thermophys.* **83** (3), 513–524.

COMBEST, D. P., RAMACHANDRAN, P. A. & DUDUKOVIC, M. 2011 On the gradient diffusion hypothesis and passive scalar transport in turbulent flows. *Ind. Engng Chem. Res.* **50** (15), 8817–8823.

DUTTA, A. & TARBELL, J. M. 1989 Closure models for turbulent reacting flows. *AIChE J.* **35** (12), 2013–2027.

FABREGAT, A., PALLARÈS, J., CUESTA, I. & GRAU, F. X. 2010 Numerical simulations of a second-order chemical reaction in a plane turbulent channel flow. *Intl J. Heat Fluid Flow* **53**, 4248–4263.

FENG, H., OLSEN, M. G., HILL, J. C. & FOX, R. O. 2007 Simultaneous velocity and concentration field measurements of passive-scalar mixing in a confined rectangular jet. *Exp. Fluids* **42** (6), 847–862.

FENG, H., OLSEN, M. G., LIU, Y., FOX, R. O. & HILL, J. C. 2005 Investigation of turbulent mixing in a confined planar-jet reactor. *AIChE J.* **51** (10), 2649–2664.

FLESCH, T. K., PRUEGER, J. H. & HATFIELD, J. L. 2002 Turbulent Schmidt number from a tracer experiment. *Agric. Forest Meteorol.* **111** (4), 299–307.

FOX, R. O. 2003 *Computational Models for Turbulent Reacting Flows*. Cambridge University Press.

HANAZAKI, H. & HUNT, J. C. R. 1996 Linear processes in unsteady stably stratified turbulence. *J. Fluid Mech.* **318**, 303–337.

HILL, J. C. 1976 Homogeneous turbulent mixing with chemical reaction. *Annu. Rev. Fluid Mech.* **8**, 135–161.

KOMORI, S., KANZAKI, T. & MURAKAMI, Y. 1994 Concentration correlation in a turbulent mixing layer with chemical reactions. *J. Chem. Engng Japan* **27** (6), 742–748.

KOMORI, S. & NAGATA, K. 1996 Effects of molecular diffusivities on counter-gradient scalar and momentum transfer in strongly stable stratification. *J. Fluid Mech.* **326**, 205–237.

KOMORI, S., NAGATA, K., KANZAKI, T. & MURAKAMI, Y. 1993 Measurements of mass flux in a turbulent liquid flow with a chemical reaction. *AIChE J.* **39** (10), 1611–1620.

LIBBY, P. A. & BRAY, K. N. C. 1981 Countergradient diffusion in premixed turbulent flames. *AIAA J.* **19** (2), 205–213.

LIGNELL, D. O., CHEN, J. H. & SCHMUTZ, H. A. 2011 Effects of Damköhler number on flame extinction and reignition in turbulent non-premixed flames using DNS. *Combust. Flame* **158** (5), 949–963.

MELL, W. E., NILSEN, V., KOSÁLY, G. & RILEY, J. J. 1994 Investigation of closure models for nonpremixed turbulent reacting flows. *Phys. Fluids* **6**, 1331–1356.

MIZOBUCHI, Y., SHINJO, J., OGAWA, S. & TAKENO, T. 2005 A numerical study on the formation of diffusion flame islands in a turbulent hydrogen jet lifted flame. *Proc. Combust. Inst.* **30** (1), 611–619.

NAGATA, K. & KOMORI, S. 2000 The effects of unstable stratification and mean shear on the chemical reaction in grid turbulence. *J. Fluid Mech.* **408**, 39–52.

NAKAMURA, I., SAKAI, Y. & MIYATA, M. 1987 Diffusion of matter by a non-buoyant plume in grid-generated turbulence. *J. Fluid Mech.* **178**, 379–403.

NISHIKI, S., HASEGAWA, T., BORGHI, R. & HIMENO, R. 2006 Modelling of turbulent scalar flux in turbulent premixed flames based on DNS databases. *Combust. Theor. Model.* **10** (1), 39–55.

PATTERSON, G. K. 1981 Application of turbulence fundamentals to reactor modelling and scaleup. *Chem. Engng Commun.* **8**, 25–52.

PITSCH, H. 2006 Large-eddy simulation of turbulent combustion. *Annu. Rev. Fluid Mech.* **38**, 453–482.

POPE, S. B. 2000 *Turbulent Flows*. Cambridge University Press.

SAWFORD, B. L. 2006 Lagrangian stochastic modelling of chemical reaction in a scalar mixing layer. *Boundary-Layer Meteorol.* **118** (1), 1–23.

SHEPHERD, I. G., MOSS, J. B. & BRAY, K. N. C. 1982 Turbulent transport in a confined premixed flame. *Nineteenth Symp. (Intl) on Combustion*, pp. 423–431. The Combustion Institute.

TENNEKES, H. & LUMLEY, J. L. 1972 *A First Course in Turbulence*. MIT Press.

TOMINAGA, Y. & STATHOPOULOS, T. 2007 Turbulent Schmidt numbers for CFD analysis with various types of flowfield. *Atmos. Environ.* **41** (37), 8091–8099.

TOOR, H. L. 1969 Turbulent mixing of two species with and without chemical reactions. *Ind. Engng Chem. Fundam.* **8** (4), 655–659.

TOOR, H. L. 1993 Effect of chemical reactions on turbulent diffusivities. *AIChE J.* **39** (10), 1603–1610.

VEYNANTE, D., TROUVÉ, A., BRAY, K. N. C. & MANTEL, T. 1997 Gradient and counter-gradient scalar transport in turbulent premixed flames. *J. Fluid Mech.* **332**, 263–293.

VEYNANTE, D. & VERVISCH, L. 2002 Turbulent combustion modeling. *Prog. Energy Combust. Sci.* **28** (3), 193–266.

WANG, D. M. & TARBELL, J. M. 1993 Closure models for turbulent reacting flows with a nonhomogeneous concentration field. *Chem. Engng Sci.* **48** (23), 3907–3920.

WATANABE, T., SAKAI, Y., NAGATA, K. & TERASHIMA, O. 2013 Joint statistics between velocity and reactive scalar in a turbulent liquid jet with a chemical reaction. *Phys. Scr.* T **155**, 014039.

WATANABE, T., SAKAI, Y., NAGATA, K., TERASHIMA, O. & KUBO, T. 2012 Simultaneous measurements of reactive scalar and velocity in a planar liquid jet with a second-order chemical reaction. *Exp. Fluids* **53** (5), 1369–1383.

YIMER, I., CAMPBELL, I. & JIANG, L. Y. 2002 Estimation of the turbulent Schmidt number from experimental profiles of axial velocity and concentration for high-Reynolds-number jet flows. *Can. Aeronaut. Space J.* **48** (3), 195–200.